Particle-size dependence of magnetization relaxation in Mn_{12} crystals

Neus Domingo,[1] Fernando Luis,[2] Motohiro Nakano,[3] Maria Muntó,[4] Jordi Gómez,[4] Jesús Chaboy,[2] Nora Ventosa,[4] Javier Campo,[2] Jaume Veciana,[4] and Daniel Ruiz-Molina[1]

[1]*Centre d'Investigació en Nanociència i Nanotecnologia (ICN-CSIC), Campus UAB, 08193 Cerdanyola del Vallès, Spain*

[2]*Departamento de Física de la Materia Condensada and Instituto de Ciencia de Materiales de Aragón, CSIC-Universidad de Zaragoza, 50009 Zaragoza, Spain*

[3]*Department of Applied Chemistry, Graduate School of Engineering, Osaka University, 2-1 Yamada-oka, Suita 565-0871, Japan*

[4]*Institut de Ciència de Materials de Barcelona (CSIC), Networking Research Center on Bioengineering Biomaterials and Nanomedicine (CIBER-BBN), Campus UAB, 08193 Cerdanyola del Vallès, Spain*

(Received 31 December 2008; published 5 June 2009)

We show that reducing the crystal size of $[Mn_{12}O_{12}(O_2C_6H_5)_{16}(H_2O)_4]$ single-molecule magnets from 11.5 to 0.4 μm strongly affects the molecular magnetic anisotropy and magnetic-relaxation rates. The effective activation energy for the spin reversal of the standard clusters decreases by 13% with decreasing size, whereas it remains approximately constant for the "fast relaxing" species. The pre-exponential factor τ_0 increases with decreasing crystal size for both. The observed decrease in the effective energy barrier for the slow relaxing species seems to be associated with the existence of a distribution of second-order transverse anisotropy terms, centered on $E=0$, which broadens as the crystal size decreases. By contrast, the expected changes in the axial anisotropy parameter D with decreasing crystal size are too small to account for the change in U. The different effects that the reduction in crystal size has on the fast and slow relaxing species are discussed.

DOI: 10.1103/PhysRevB.79.214404 PACS number(s): 75.30.Gw, 75.50.Xx, 75.50.Tt, 78.70.Dm

I. INTRODUCTION

Manganese oxide clusters of general formula $[Mn_{12}O_{12}(RCOO)_{16}(H_2O)_4]$ (Mn_{12}; R=alkyl and aryl) show a remarkable single-molecule magnet (SMM) behavior.[1] The combination of high-spin and strong uniaxial magnetic anisotropy leads to slow magnetic relaxation and hysteresis at low temperatures. In addition, they show intriguing quantum behavior such as quantum tunneling between their spin-up and spin-down states, which can be turned on and off by the application of magnetic fields.[2]

A qualitative account for all these phenomena can be achieved with the simplest model of the ideal isolated molecule. However, a quantitative description is much more complex and involves the interaction with the environment. For instance, such interaction can induce and modulate the off-diagonal terms in the Hamiltonian (i.e., not commuting with the spin projection S_z along the anisotropy axis) that account for the quantum-tunneling magnetization in these molecules.[3–5] Moreover, the influence of the environment turns out to be decisive for the appearance of a second species of Mn_{12} molecules showing faster relaxation. This species has been associated with the presence of an anomalous Jahn-Teller distortion.[6–8]

For this reason, several studies have been carried out over the last few years to understand the interaction of the SMM with the medium and how it can influence their magnetization relaxation and the quantum tunneling of magnetization (QTM). For example, SMMs have been incorporated into porous silica, surfaces, polymers, and Langmuir Blodgett films, among others.[9] It has also become evident that disorder plays a non-negligible role in determining the tunneling rates and the energy splitting between magnetic energy levels. Essentially, two sources of disorder have been considered. First, the disorder that arises from lattice defects such as dislocations.[3,4] And second, the disorder induced by the local orientation of interstitial molecules from the crystallization process.[5]

The preparation of crystalline samples of SMMs with controlled structural parameters, such as morphology, size, and crystallographic phase, will represent an excellent scenario to study the influence of these structural parameters on the magnetization relaxation mechanisms. For this, conventional crystallization methods are not suitable since they show a very limited control over particle size and crystal phase of the final material. These solvent-based processes are driven by temperature or by changes in the composition of the solvent evaporation, addition of antisolvents, and addition of salts, which are slowly and nonhomogeneously transmitted in liquid media. To avoid this problem, new approaches based on a fast precipitation method have been recently developed. Metal-organic sub-50-nm spherical particles that exhibit SMM behavior have been fabricated by direct precipitation of Mn_{12} clusters in a mixture of acetonitrile and toluene.[10] A complementary approach is based on the use of compressed fluids (CFs). In their liquid or supercritical state, they can be tuned by pressure changes that propagate much more quickly and homogeneously than temperature and composition solvent changes. Therefore, compressed solvents enable a much higher control and tuning of the structural characteristics of the final material (size, porosity, polymorphic nature, morphology, etc.) than liquid solvents and often lead to materials with unique physicochemical characteristics unattainable by conventional processing methods.[11]

Recently, new crystallization procedures based on the use of CFs as solvent media have been shown to be very effective for the straightforward preparation of Mn_{12} crystalline solids with microscopic or nanoscopic particle size, smaller size dispersion, and high crystallographic phase purity.[12] Our previous work describes the synthesis method and how it

enables a good control over the crystal morphology and size. Details about the morphological and crystallographic characterization are also given there.[12] In the present work we focus on studying how these parameters influence the magnetization relaxation and quantum tunneling of Mn_{12} single-molecule magnets. For this, we have concentrated on the study of the magnetization-relaxation phenomena of a set of crystalline samples with sizes ranging from 11.5 to 0.4 μm of $[Mn_{12}O_{12}(O_2C_6H_5)_{16}(H_2O)_4]$ (Mn12bz, complex **1**) prepared by using supercritical fluids.[12] The lack of interstitial molecules of complex **1** is especially appealing in order to study pure effects of the crystal size.

The organization of the paper is as follows: in Sec. II we describe the sample's characterization and in Sec. III A we present the results for the structural characterization followed by the results for the ac magnetic characterization in Sec. III B. Finally, results are discussed in Sec. IV and compared with numerical simulations, and conclusions are given in Sec. V.

II. SAMPLE PREPARATION AND CHARACTERIZATION

Crystallization of complex **1** by the aerosol solvent extraction system (ASES) technique using $CHCl_3$ as organic solvent is already explained in a previous work.[12,13] Four different samples of complex **1** with different mean particle diameters, 11.5 (**1**a), 5.8 (**1**b), 1.1 (**1**c), and 0.4 μm (**1**d), were obtained by different ASES crystallization experiments carried out at the same constant temperature, pressure, and supersaturation ratio but different CO_2 concentrations (X_{CO2}).[12] Varying X_{CO2} enables a good control over the average particle size. Particle-size distributions were measured using a laser diffraction analyzer whereas the morphology of the crystals was examined by using scanning electron microscopy. The average particle size is smaller than that obtained for this material when it is crystallized by conventional diffusion techniques, and the samples show a higher uniformity index. X-ray powder spectra were measured on samples placed into a 300-μm-diameter capillary and recording the spectra from $2\theta=2°$ to $2\theta=60°$.

X-ray absorption spectroscopy experiments were performed at the beamline BL39XU of the SPring8 Facility.[14] X-ray absorption near-edge structure (XANES) spectra were recorded at room temperature in the transmission mode at the *K* edge of Mn. The undulator radiation was monochromatized by a diamond (111) fixed-exit double-crystal monochromator. Higher harmonics were rejected by a Rh-coated mirror. For the measurements, homogeneous layers of the powdered samples were made by spreading fine powders of the material on an adhesive tape. The thickness and homogeneity of the samples were optimized to achieve the best signal-to-noise ratio, giving a total absorption edge jump of $\sim$1. The absorption spectra were analyzed according to standard procedures.[15] The origin of the energy scale was chosen at the inflection point of the absorption edge, and the spectra were normalized to the averaged absorption coefficient at high energy in order to eliminate the dependence of the absorption on samples thickness.

ac susceptibility data were measured in a Quantum Design superconducting quantum interference device magnetometer between 0.01 and 1.4 kHz, with a 3.0 Oe ac oscillating magnetic field, and also under the presence of external dc magnetic fields. Above 100 Hz, the susceptibility was measured with a Physical Properties Measurement System (PPMS) experimental platform that uses a conventional inductive method. In all cases, samples were mixed with grease to avoid the rotation of the powder grains under external magnetic fields up to 3000 Oe. The contributions of the grease and sample holder were measured separately and subtracted from the data.

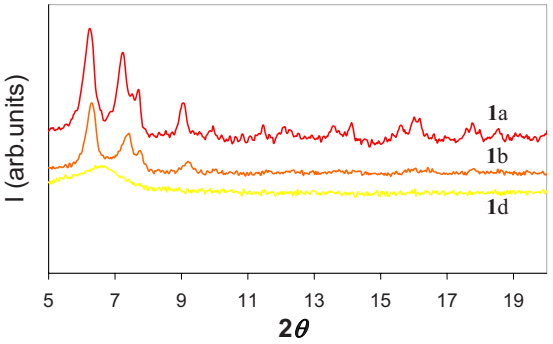

FIG. 1. (Color online) X-ray spectra for samples **1**a (top, red), **1**b (middle, orange), and **1**d (bottom, yellow).

III. RESULTS

A. Structural characterization

From the study of the x-ray powder diffractograms of the different samples of complex **1** processed by the ASES method (Fig. 1), we observe that the crystalline phase obtained for samples **1**a and **1**b is in agreement with the previously published structure,[16] consisting on orthorhombic crystal systems of the *Fdd*2 space group. For the sample with the smallest crystal size, **1**d, the diffractogram shows a broad peak centered near $2\theta=6.5°$ suggesting that this sample is amorphous. The broadening of the reflections measured on sample **1**b with respect to those observed for sample **1**a, which contains the largest crystals, also suggests a certain increase in the density of defects in the crystals, induced during the first stages of the fast crystallization process. This might lead to an increase in the mosaicity of the crystals for decreasing crystal size, which for the smallest sizes would just look amorphous. However, no quantitative analysis can be extracted from the available data.[4]

In order to get a deeper insight on the origin of the changes observed in the magnetic properties, we have investigated by x-ray absorption spectroscopy methods how the local environment of the Mn sites is affected by changes in the crystal size. Reliable structural parameters are commonly derived from the analysis of the extended x-ray absorption fine structure (EXAFS) region of the spectrum. However, in the present case, the accuracy of the structural determination obtained by EXAFS gets involved due to the presence of equivalent crystallographic sites and different electronic states for the Mn atoms. Instead, the XANES part of the absorption spectrum shows a great sensitivity to the bonding geometry of the absorbing site (overall symmetry, distances,

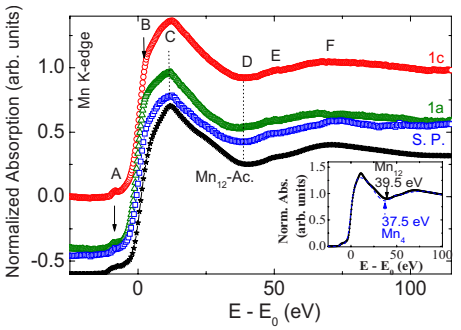

FIG. 2. (Color online) Normalized Mn *K*-edge XANES spectrum of samples **1**a (red circles) and **1**c (green triangles) compared with the spectra of the starting product (blue squares) and of crystalline Mn_{12} acetate (black stars). The inset shows the normalized absorption spectrum for crystalline Mn_{12} acetate (black straight line) and Mn_4 cubane (dashed blue line) as explained in the text.

and bond angles). Therefore, we have studied the Mn *K*-edge XANES to determine how the Mn-O distances depend on the crystal size.

Results of the XANES measurements performed at the Mn *K* edge in the case of samples **1**a and **1**c are shown in Fig. 2. These spectra are compared to those of the precursor (starting product) and of crystalline Mn_{12} acetate. As shown in the figure, no significant differences are found between the spectra. Indeed, all the Mn *K*-edge spectra are characterized by the existence of a prepeak (A) and a broad and asymmetric main absorption line which shows a bump (B) at low energies. The maximum of the main line (C) lies in all cases at ~11 eV above the edge. Moreover, all the compounds show a dip (D) at ~38 eV, a weak but well-defined peak (E) at ~50 eV, and a broad structure at higher energies (F) centered at about 70 eV above the edge. Therefore no significant modification of the XANES spectra, neither in shape nor in amplitude, is observed down to 0.5 eV, and the different spectral features occur at the same energy values in all samples. These results show that any change in the local coordination of the Mn ions induced by either varying the crystal's size or the method of synthesis must be smaller than the experimental resolution of 0.03 Å.

In order to illustrate how the modification of the interatomic distances affects the spectral shape, the energy position of the different spectral features, and their intensity ratio, we have compared, in the inset of Fig. 2, the Mn *K*-edge spectra of Mn_{12} acetate and of $Mn_4O_3(OAc)_4(dbm)_3$. Both compounds exhibit similar Mn-O environments, with the main difference being that while in the case of Mn_{12} acetate the longest Mn-O bond is 2.24 Å, it is 2.3 Å in the case of the Mn_4 cubane. As shown in the inset, the energy position of the absorption minimum D is shifted by 2 eV between the cubane (37.5 eV) and the acetate (39.5 eV) spectra. According to Natoli's rule, which determines the inverse relationship existing between absorption energy and the interatomic distance,[17] this shift implies that the Mn-O bonds are on average shorter in the acetate than in the cubane. In this way the peak energies on a XANES spectrum can be linked empirically to the Mn-O distances through the simple relationship $(E-E_0)R^2=$const, where E and R are the peak energy and corresponding Mn-O distance, whereas E_0 is an energy close to the onset of the edge. Applying this rule to the minima of the Mn_{12} acetate and Mn_4 cubane spectra yields a ratio of 1.026 between the Mn-O distances in the two compounds, which is in perfect agreement with the ratio between the longest Mn-O bonds. Finally, it should be also noted that the edge position is intimately linked to the local structure. For instance, when the bond length of a molecule becomes longer, the position of the edge shifts to lower energy.[18] As shown in Fig. 2, no shift of the edge is observed between the spectra of crystalline Mn_{12} acetate and samples **1**a and **1**c. These results point out that no modification of the local environment of the Mn ions is produced by varying the size of the crystal or the method of synthesis.

B. Frequency-dependent susceptibility

ac susceptibility data measured on samples **1**a–**1**d at eight different frequencies as a function of temperature are shown in Fig. 3. Two peaks corresponding to superparamagnetic freezing are seen for both the in-phase component χ' and the out-of-phase component χ'' of the ac susceptibility. The blocking temperature T_B, defined as the temperature of maximum χ'', increases with the frequency ω of the ac field. The two peaks are associated with the presence of two different Mn_{12} species with different magnetic anisotropies, as observed for most of the Mn_{12} derivatives.[6–8,19] In the slow relaxing (SR) molecules with the higher T_B, the elongated Jahn-Teller axes of the Mn^{3+} ions are all nearly parallel to the molecular axis of Mn_{12} molecule, while for the fast relaxing (FR) molecules one of the Mn^{3+} ions has an unusual Jahn-Teller distortion.[8] Well above T_B, the in-phase component of the ac susceptibility (χ') achieves its equilibrium value χ_{eq} that is observed to obey the Curie-Weiss law

$$\chi_{eq} = N_A \frac{g^2 \mu_B^2 S^2}{3k_B(T-\theta)} = \frac{C}{(T-\theta)}. \quad (1)$$

By fitting this equation to the $\chi'(T)$ data for temperatures above the two blocking peaks (see Fig. 3), it is possible to obtain the relative fractions of FR (f_{FR}) and SR ($1-f_{FR}$) molecules. The values for f_{FR} obtained in this way are shown in Table I and range from 44% to 62%. The obtained Weiss temperatures θ show the existence of weak antiferromagnetic interactions between different single-molecule magnets due to dipolar interactions. Notice that $\theta \ll T_B$, which justifies the use of Eq. (1). These parameters do not show any systematic and important change with size.

Let us consider next the spin dynamics for the different samples. As a first approximation, the average relaxation time τ for the reversal of the molecular spins can be estimated by assuming that the blocking temperature corresponds to the condition $\omega\tau=1$. In Fig. 4(a), we compare $\chi''(T)$ experimental curves measured at a fixed frequency of $\omega=90$ Hz on samples with average diameters ranging from 11 down to 0.4 μm. The blocking temperatures extracted from them are plotted in Fig. 4(b) as a function of size. These data reveal clear changes in the spin dynamics that are apparently induced by the decrease in size: the blocking temperature decreases by 6% in the case of the standard or slow

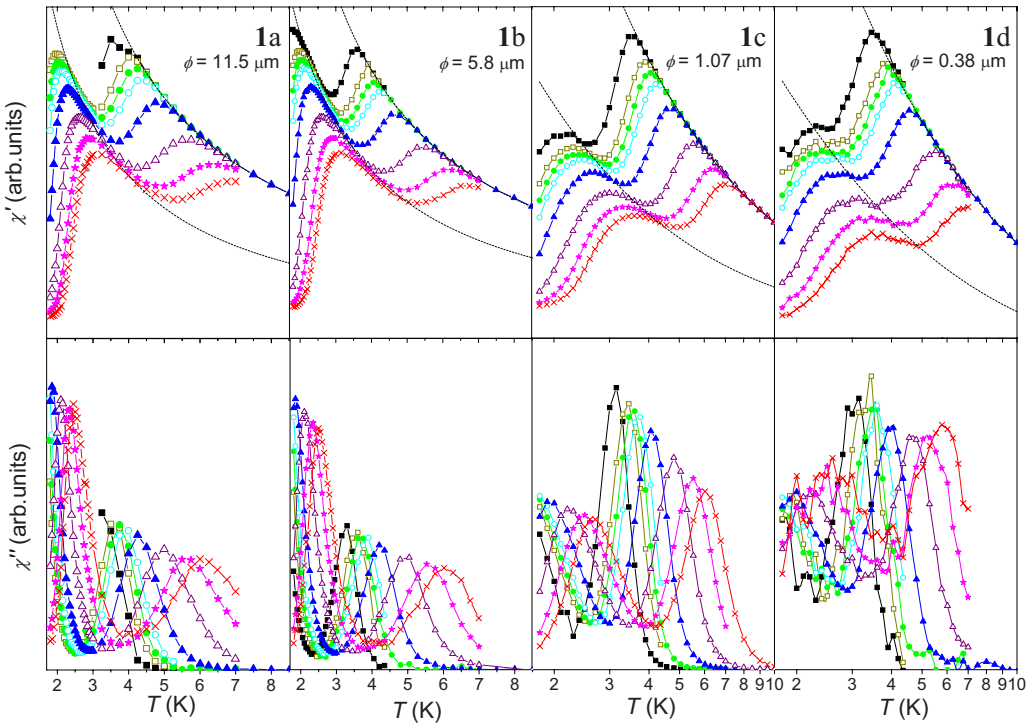

FIG. 3. (Color online) Temperature dependence of the ac magnetic susceptibility for the four samples of complex **1**, at eight different frequencies: 0.1 (■, black), 0.5 (□, dark yellow), 1 (●, green), 2 (○, cyan), 9 (▲, blue), 90 (△, purple), 476 (★, magenta), and 1380 Hz (×, red). Top: in-phase component of the magnetic susceptibility and bottom: out-of-phase component of the magnetic susceptibility. The dash lines correspond to the fitting of the Curie-Weiss law above the blocking temperatures [Eq. (1)].

relaxing molecules whereas it increases by the same relative amount for the fast relaxing ones.

The relaxation to equilibrium is determined by the height of the anisotropy energy barrier, the rates of tunneling across this barrier, and the strength of the spin-phonon interaction. We shall try next to identify which of these factors are being affected by the reduction in size for each of the two Mn_{12} species. In the thermally activated tunneling range, that is, for not too low temperatures, the relaxation time τ is well described by the Arrhenius law

$$\tau_i(T) = \tau_{0,i} \exp\left(\frac{U_i}{k_B T}\right) \tag{2}$$

for i=FR and SR since here we apply it independently to describe the fast or slow relaxation species. By fitting Eq. (2) to the data of ln ω vs $(1/T_B)$, we can obtain the activation energy U and the pre-exponential time scales τ_0 for the SR and FR species of all samples, as shown in Fig. 5. These parameters are listed in Table II.

TABLE I. Particle sizes of samples of complex **1** and parameters of the fitting of Curie law [Eq. (1)] to the data, where f_{FR} is the fraction of the FR species and θ is the Weiss temperature.

Sample	Size (μm)	U.I.[a]	f_{FR}	θ (K)
1a	11.5	15	0.57 ± 0.05	-0.32 ± 0.02
1b	5.80	29	0.62 ± 0.03	-0.25 ± 0.03
1c	1.07	66	0.44 ± 0.03	-0.30 ± 0.02
1d	0.38	77	0.48 ± 0.06	-0.38 ± 0.04

[a]Uniformity index is defined as U.I.$=D[v,0.1]/D[v,0.9]\times 100$ and describes the polydispersity of the system.

Figure 6 shows how τ_0 and U depend on the average particle's size. For the two species of Mn_{12}, we observe τ_0 increasing with decreasing size. Since τ_0 depends on the lifetime of the excited spin-energy levels, this increase indicates that spin-lattice interactions become weaker. This effect was not observed in nanoparticles of Mn_{12} prepared by direct precipitation of Mn_{12} clusters for which τ_0 was found to be shorter than in bulk.[10] It suggests that the fast crystallization process employed here leads to a hardening of the crystal lattice (or more specifically, to a larger average speed of sound) with respect to the bulk. As for the activation energy, it is found to remain nearly constant within experimental uncertainties for the FR species (see the Arrhenius plots of Fig. 5) whereas for the SR species it shows a monotonic decrease with decreasing crystal's size. In the latter case, this decrease more than compensates for the increase in $\tau_{0,SR}$ and it is therefore responsible for the observed decrease in the blocking temperature.

Although, as a first approximation, we can characterize the magnetic relaxation by the average relaxation time, in a crystal made of single-molecule magnets we rather have to consider a distribution of relaxation times. The distribution arises from inhomogeneities in the dipolar magnetic fields or from molecular imperfections or distortions. All of these can be affected by a reduction in crystal's size. Information on this distribution can be obtained from the dependence of the

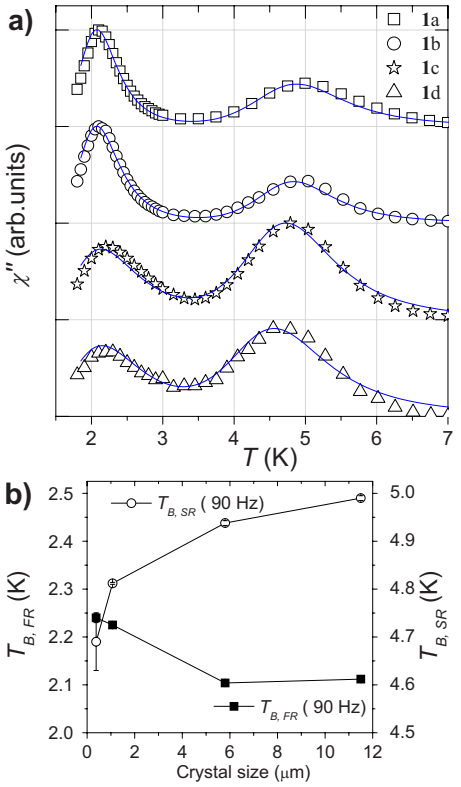

FIG. 4. (Color online) (a) Out-of-phase ac magnetic susceptibility for all samples at a single frequency of 90 Hz. The straight solid blue lines correspond to the fitting curves with Eq. (4) using the parameters of Tables I and II as explained in the text. (b) Peak position as a function of the average crystal's size for the SR and the FR species of complex **1**.

ac magnetic susceptibility on frequency measured at fixed temperatures. Typically, the in-phase component $\chi'(\omega)$ of the ac magnetic susceptibility attains its equilibrium value at low frequencies whereas it decreases toward the adiabatic susceptibility at high frequencies. The drop in $\chi'(\omega)$ is accompanied by a symmetric peak in the out-of-phase susceptibility $\chi''(\omega)$. The behavior found for the Mn_{12} microcrystals is complicated by the presence of two species characterized by very different relaxation times, but it can nevertheless be

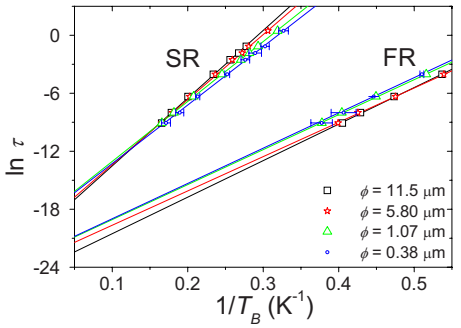

FIG. 5. (Color online) Arrhenius law fitting for the FR and the SR species of complexes **1**a (black squares), **1**b (red stars), **1**c (green triangles), and **1**d (blue circles). The error bars correspond to the size of the symbol except for complex **1**d, which are shown separately.

understood on the same qualitative basis. Figure 7 shows $\chi^*(\omega)$ at three different temperatures for sample **1**a. At 2.0 K only the relaxation of the fast relaxation species contributes to the frequency dependence since the SR molecules, with higher blocking temperature, are still completely blocked at this frequency range. By contrast, at 4.8 K, the frequency dependence of the ac susceptibility is mainly dominated by the SR species since the FR molecules remain in equilibrium even at the highest frequency of 1.4 kHz. In the intermediate regime of around 3.5 K and low frequencies, we observe the contribution to χ'' arising from the progressive blocking of the two species: the SR at low frequencies and the FR in the high-frequency region above 100 Hz. This intermediate regime is also clearly observed in the Argand plots (χ'' vs χ') (inset of Fig. 7). While for 2 and 5 K a single semicircle is observed, for temperatures in between, two pieces of two different semicircles are clearly seen.

In order to get a more quantitative analysis of these experimental data, we use the Cole-Cole phenomenological expression for the complex susceptibility χ^*, which replaces the Debye law when a distribution of relaxation times is present in the sample,

$$\chi^*(\omega,T) = \chi_\infty + \frac{\chi_{eq} - \chi_\infty}{1 + (i\omega\tau)^{1-\alpha}}. \tag{3}$$

Here, $\tau(T)$ is the average relaxation time described by the Arrhenius law [Eq. (2)] and the factor $0 < \alpha \leq 1$ accounts for the distribution of relaxation processes as it measures the width of the distribution (for $\alpha=0$, we recover the Debye-type relaxation defined by a single relaxation time). We can see the influence of the parameter α as a flattening of the characteristic perfect semicircle shown for the Argand plots of a Debye relaxation system (inset of Fig. 7). $\chi_{eq}(\omega \to 0)$ is the equilibrium susceptibility and $\chi_\infty(\omega \to \infty)$ is the adiabatic limit of the susceptibility. In order to consider the different relaxation mechanisms accounting for the two observed peaks, two different Cole-Cole equations are considered for the FR and the SR species, respectively,

$$\chi^*_{\text{total}}(\omega,T) = \chi_\infty + \chi(T)\left[f_{\text{FR}}\frac{1}{1 + (i\omega\tau_{\text{FR}})^{1-\alpha_{\text{FR}}}} + (1 - f_{\text{FR}})\frac{1}{1 + (i\omega\tau_{\text{SR}})^{1-\alpha_{\text{SR}}}}\right]. \tag{4}$$

This equation was fitted to the frequency-dependent measurements of the ac susceptibility to obtain the parameter α for each species. To avoid overparametrization, the fraction of fast relaxation species (f_{FR}), $\tau_i(T)$, and $\chi(T)$ were fixed. The values of f_{FR} were obtained with the Curie law as explained before (Table I) whereas the values of $\tau_i(T)$ were calculated from the U_i and $\tau_{0,i}$ values already obtained from the fittings of the Arrhenius law (Table II). The temperature-dependent susceptibility term $\chi(T)$ included in Eq. (4) was replaced with the Curie law [Eq. (1)] as previously fitted to the thermal dependence of the $\chi'(T)$ for $T > T_B$. An illustrative example of the resulting fitting curves obtained is shown in Fig. 4(a). The values obtained for the parameter $\alpha_{\text{FR, SR}}$ shown in Fig. 6 evidence a strong broadening of the energy-

TABLE II. Parameters obtained in the fitting of Arrhenius law [Eq. (2)] and the Cole-Cole equation [Eq. (5)] to the susceptibility data of all samples.

		SR			FR		
Sample	Size (μm)	U_{SR}/k_B (K)	τ_{SR} (ns)	α_{SR}	U_{FR}/k_B (K)	τ_{FR} (ns)	α_{FR}
1a	11.5	70.1 ± 1.0	7.7 ± 0.6	0.29 ± 0.02	37.8 ± 1.0	0.17 ± 0.07	0.41 ± 0.04
1b	5.80	67.3 ± 0.9	11.6 ± 0.4	0.19 ± 0.01	35.5 ± 0.8	0.53 ± 0.12	0.42 ± 0.02
1c	1.07	62.0 ± 0.3	27.5 ± 0.9	0.25 ± 0.01	36.2 ± 0.5	0.88 ± 0.24	0.61 ± 0.02
1d	0.38	60.5 ± 2.2	25.6 ± 14	0.31 ± 0.02	36.5 ± 1.7	0.94 ± 0.75	0.64 ± 0.04

barrier distribution of the FR species on decreasing crystal's size, as it is qualitatively observed in Fig. 4(a). In contrast, the parameter α_{SR} shows values in the range of 0.2–0.3, lacking any correlation with size within experimental uncertainties.

IV. DISCUSSION

From the results presented in the previous section, it follows that the magnetic properties of Mn_{12} clusters prepared by the use of compressed fluids depend on the average size of the crystal. A rather unexpected finding is the observed decrease in U_{SR} with decreasing size since the anisotropy is considered to be a property of each individual molecule. In addition, the surface-to-volume ratio remains very small, on the order of 2% or less, even for the smallest crystals considered in the present study. Therefore, when considering the size effects, we might safely rule out the modification of surface clusters as a plausible explanation of our results and look for an alternative. As will be argued below, the changes observed are probably caused mainly by the modification of the perfect crystalline structure and the stresses induced at the early stages of the fast crystallization process.

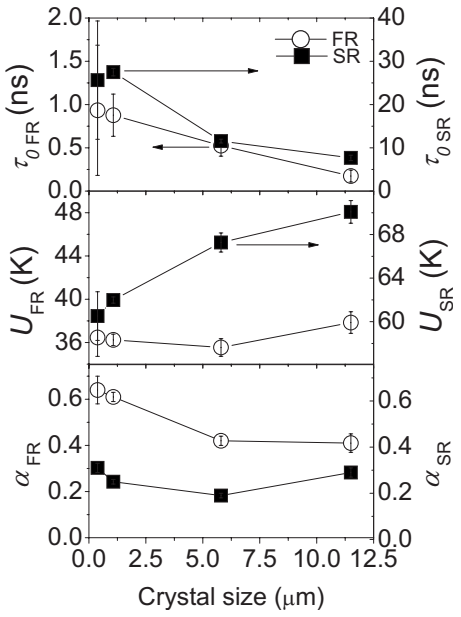

FIG. 6. Particle-size dependence of the different parameters describing the magnetic relaxation of Mn_{12} clusters. Top panel: effective energy barrier $U_{SR,FR}$. Medium panel: characteristic relaxation time $\tau_{0,SR,FR}$. Values corresponding to the FR (■) molecules are given on the left-hand axis while those corresponding to the SR species (○) are given on the right-hand axis. Bottom panel: parameter $\alpha_{FR,\ SR}$.

The activation energy is determined by two counterbalancing factors: the total height of the anisotropy energy barrier, on one hand, and the probability of tunneling processes, on the other hand, which tend to establish a kind of shortcut of this barrier near zero field. Since tunneling is only effective under sufficiently weak bias magnetic fields, a way of shedding some light onto the decrease in U_{SR} with size is by measuring the activation energy as a function of magnetic field. For this, we carried out measurements of χ^* as a function of frequency and applied magnetic field up to 2000 Oe on samples **1**a–**1**c. As a first approximation, we can neglect the distribution of relaxation times to get an estimate of τ from the following expression:

$$\omega\tau(H) = \frac{\chi''(\omega,H)}{\chi'(\omega,H) - \chi'(\infty,H)}. \tag{5}$$

Here $\chi'(\infty,H)$ was taken as the data measured, for each magnetic field, at the highest experimental frequency of 1380 Hz. The experiments were performed at a temperature of 4 K, for which the fast relaxing species does not contribute to the variation in χ^* with frequency, as described before. From the so-obtained relaxation times, and making use of the Arrhen-

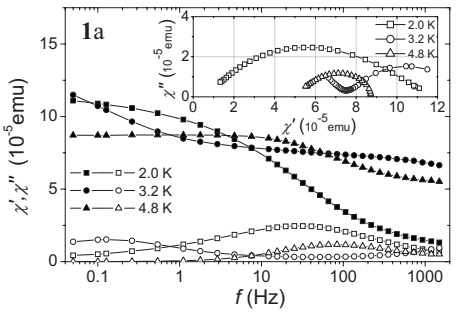

FIG. 7. Frequency dependence of the ac magnetic susceptibility for sample **1**a, at three different temperatures. Filled signals correspond to the in-phase component and empty signals correspond to the out-of-phase signal. The inset shows the Argand plot of the ac magnetic susceptibility of sample **1**a.

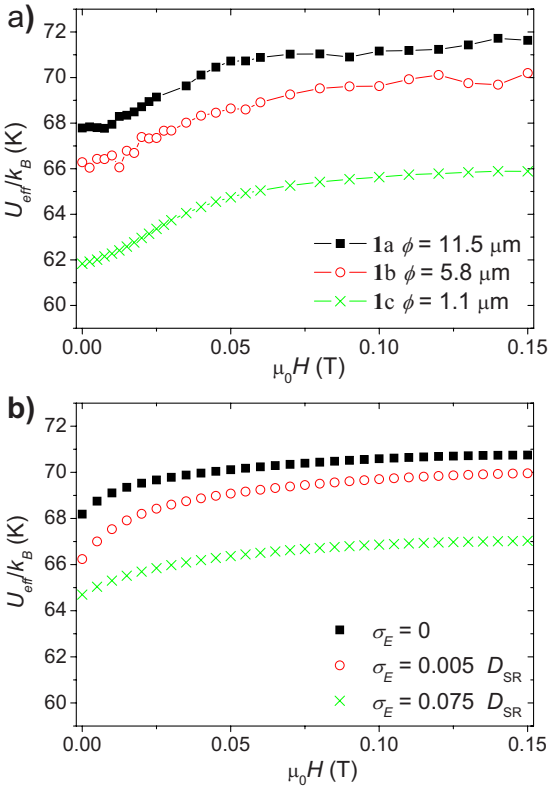

FIG. 8. (Color online) (a) Field dependence of the activation energy calculated from Eq. (6) using experimental data of the field dependence of the ac magnetic susceptibility. (b) The same calculation performed on the basis of the numerical simulation of the field dependence of the magnetic susceptibility as explained in the text.

ius law [Eq. (2)], we can estimate the behavior of the energy barrier as a function of the applied magnetic field,

$$U(H) = T \ln\left[\frac{1}{\omega\tau_0}\frac{\chi''(\omega,H)}{\chi'(\omega,H)-\chi'(\infty,H)}\right]. \quad (6)$$

Figure 8(a) shows the values $U(H)$ obtained for the samples **1**a–**1**c, from $\chi^*(H)$ data measured at $\omega/2\pi=1$ Hz. Near zero field, the activation energy is lowered by the possibility of flipping the spin via a quantum-tunneling process. However, as the magnetic field is increased, the tunneling becomes progressively blocked and the activation energy approaches gradually the classical barrier, equal to the total anisotropy barrier. The direct comparison of data measured on samples of different size [as shown in Fig. 8(a)] indicates that the differences between the activation energies found at zero field do not disappear with increasing H. In fact, the initial difference between the effective energy barriers is maintained almost constant for all the fields up to $\mu_0 H=0.15$ T. This means that such differences are not just caused by the spins tunneling via lower-lying states for samples of decreasing size but by intrinsic and significant changes in the anisotropy parameters.

The Hamiltonian for Mn_{12} can be written up to fourth order in S_z as follows:[20]

$$\mathcal{H} = \mu_B g S H - D S_z^2 + E(S_x^2 - S_y^2) + A_4 S_z^4 + C(S_+^4 + S_-^4), \quad (7)$$

where the axial parameters D and A_4 mainly set the height of the anisotropy energy barrier whereas off-diagonal parameters E and C arise from distortions of the pure axial symmetry and can induce quantum tunneling of the spin. The total or classical energy barrier can be estimated as $U_{cl}=(D-|E|)S^2-A_4S^4$. The variation with the size of the saturation or high-field values of $U(H)$ can therefore be due to either different axial parameters or to changes in the transverse anisotropies with decreasing crystal size.

In the case of Mn_{12} clusters, the uniaxial anisotropy parameter D is associated with the Jahn-Teller distortion of the oxygen octahedron surrounding the Mn^{3+} ions. However, no significant changes in the Mn-O distances can be found from our structural data, either obtained from x-ray diffractograms or from the EXAFS measurements. In both cases, the local environment of the Mn ions appears to be the same in all samples down to a resolution of 0.03 Å. Yet, taking the approximation of the angular overlapping model,[21] and assuming an exponential decrease in the ligand field parameters with the metal-ligand distances,[22] changes of about 2% in the length of the Mn-O bonds in the axis of the Jahn-Teller distortion can lead to changes of up to 4% in the values of the local ion anisotropy and thus to significant changes in D of about 3 K. But these changes would not be enough to explain the strong perturbation of the anisotropy from samples **1**a to **1**d that we observe. Thus, we need to look for alternative explanations for the change in magnetic anisotropy.

The obvious alternative is that the fast crystallization process by which the microcrystals are synthesized induces disorder in the structure that, in its turn, becomes a source for off-diagonal anisotropy terms. In the acetate of Mn_{12}, these terms have been attributed to the appearance of local disorder in the orientation of solvent acetic acid molecules of the crystals.[5,23] The hydrogen bonds to these molecules decrease the symmetry of the molecules and therefore enable the existence of a nonzero second-order off-diagonal anisotropy term. However, the Mn_{12} complex used in our experiments does not have any interstitial solvent molecules in the structure.[24] Therefore, we should look for other sources of disorder, such as long-range strains, caused by, e.g., lattice dislocations or other defects, appearing at the early stages of the crystallization process. Their density, as suggested by our x-ray diffraction data, is probably higher for crystals with smaller sizes. A spatial distribution of strains might lead to a distribution of molecular distortions that, according to Chudnovsky and Garanin,[3] can be described by a Gaussian distribution of the parameter E centered around $E=0$ with a width σ_E that increases with the concentration of lattice defects. This could also be associated to the observed increase in mosaicity.

In order to check the plausibility of this explanation, we have performed numerical simulations of the field- and frequency-dependent ac magnetic susceptibility, following a model described in a series of previous works.[25] The evolutions with time of the populations of exact eigenstates of the spin Hamiltonian [Eq. (7)] are calculated by solving Pauli's master equation, which includes the phonon-induced transi-

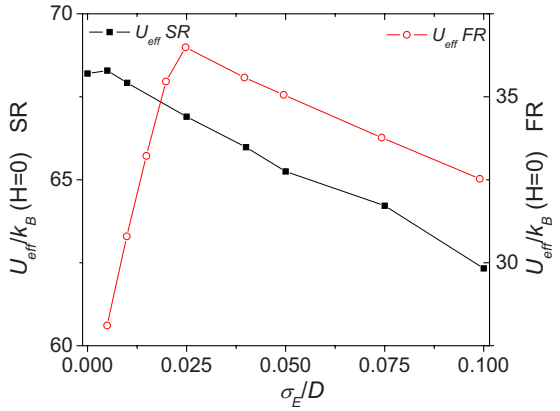

FIG. 9. (Color online) Dependence of the simulated activation energy at zero field on the width σ_E of the distribution of the E parameters. Black-filled squares correspond to the simulation for the SR species with $E=0$ K while empty red circles correspond to the simulation for the FR species with $E=0.09$ K.

tions between these eigenstates. The probabilities of tunneling are taken into account, in a natural way, via the shape of the wave functions describing such eigenstates. The model has the advantage of being applicable to situations in which strong magnetic fields are applied. We took the following values for the anisotropy parameters of the unperturbed molecules: $D=0.60$ K, $E=0$ K, $A_4=-1.0\times10^{-3}$ K, and $C=-3.0\times10^{-5}$ K, obtained from spectroscopic experiments on bulk samples,[26] and introduced the effect of dipolar interactions by an effective magnetic field with components $H_{\mathrm{dip},z}=H_{\mathrm{dip},x}=205$ Oe. We have investigated the effect of molecular distortions by introducing a Gaussian distribution of E values around $E=0$ with different σ_E values. In order to mimic the experimental procedures, we have estimated the activation energy as a function of the magnetic field by means of Eq. (6), using the calculated susceptibility values. The results of these calculations are shown in Fig. 8(b). It is clear that an increase in σ_E generates a monotonic decrease in the average activation energy either at zero or under increasing magnetic fields.

The same model can also be used to investigate the different behavior found for the two Mn_{12} species. We repeated the same simulation for the FR species, taking the parameters $D=0.45$ K, $E=0.09$ K, $A_4=2.1\times10^{-3}$ K, and $C=-2.5\times10^{-5}$ K.[8] In this case (as it is shown in Fig. 9) an initial increase in the effective energy barrier with σ_E is followed by a smooth decrease. As it is easy to understand, the relative effect that a distribution in the parameter E has on the magnetic relaxation depends on whether the original molecule already possesses an E value different from zero or not. When $E=0$, as it is probably the case for the molecules of the SR fraction, any nonzero E value induced by the molecular distortions will speed up the tunneling processes. By contrast, in the case of FR molecules, having a nonzero E parameter, there is a competition between the two effects. Some molecules will relax their spins faster and some slower, leading to a broader distribution of tunneling and relaxation rates, as observed experimentally. In other words, and contrary to the standard Mn_{12} clusters, a distribution of transverse anisotropy terms does not necessarily lead to a smaller activation energy for the spin reversal of a FR Mn_{12}.

V. CONCLUSIONS

The preparation of micron-sized crystals of Mn_{12}bz by the ASES crystallization technique that exhibit the same crystallographic phase but differ on the mean particle diameters has enabled us to study the influence of this parameter on the magnetic-relaxation processes of single-molecule magnets. The presence of two relaxation mechanisms attributed to the two Jahn-Teller isomers were observed in all the samples, being the fraction of molecules of each isomer independent of the crystal's size. The fast crystallization leads to weaker spin-lattice interactions, as observed by an increase in the prefactor τ_0 with decreasing crystal's size. Fast relaxing Mn_{12} molecules show nearly size-independent activation energies, whereas the distribution of relaxation times broadens, as the average size decreases. The standard or slow-relaxing Mn_{12} species shows, by contrast, a monotonic decrease in the effective activation energy U_{SR}. We have shown that this decrease must be related to very strong changes in the anisotropy parameters induced by the reduction in size and its corresponding influence on the crystallographic structure, the density of defects, and the presence of strains. Numerical simulations of the spin dynamics that include a distribution of the rhombic parameter E agree well with the experimental results. These simulations account for the faster relaxation observed in the case of the slow-relaxing species as well as for the different behavior found for the fast-relaxing clusters. The agreement suggests that the effects we observe might be related to molecular distortions induced by crystalline defects, whose density, as revealed by x-ray diffraction patterns, increases with decreasing crystal's size. From our EXAFS studies, we have been unable to find any clear-cut evidence for distortions in the local environment of the Mn^{3+} ions that contribute most to the magnetic anisotropy of these clusters. For this reason, we attribute the anisotropy changes to global distortions of the molecular core, such as rotations of the $Mn^{3+}(O^{2-})_6$ octahedra with respect to each other.

ACKNOWLEDGMENTS

N.D. acknowledges the Ministerio de Ciencia e Innovación of Spain for a grant under the program Juan de la Cierva. The work in Zaragoza was supported by research Grants No. MAT2006-13765-C02-02, No. CSD2007-00010, No. MAT2005-06806-C04-04, and No. MAT2008-06542-C04-01 from the Ministry of Science and Innovation. The work in CIN2 was supported by research Grant No. MAT2006-13765-C02-01. The work in ICMAB was supported by the "Plan Nacional de Investigación Científica y Desarrollo e Innovación Tecnológica" and project EMOCIONA under Grant No. CTQ2006-06333/BQU. Funding from the Iniciativa Ingenio 2010, Programa *Consolider*, and the European Network of Excellence MAGMANet is also gratefully acknowledged.

[1] R. Sessoli, D. Gatteschi, A. Caneschi, and A. Novak, Nature (London) **365**, 141 (1993); D. Gatteschi, A. Caneschi, L. Pardi, and R. Sessoli, Science **265**, 1054 (1994).

[2] J. R. Friedman, M. P. Sarachik, J. Tejada, and R. Ziolo, Phys. Rev. Lett. **76**, 3830 (1996); J. M. Hernández, X. X. Zhang, F. Luis, J. Bartolomé, J. Tejada, and R. Ziolo, EPL **35**, 301 (1996); L. Thomas, F. Lionti, R. Ballou, D. Gatteschi, R. Sessoli, and B. Barbara, Nature (London) **383**, 145 (1996).

[3] E. M. Chudnovsky and D. A. Garanin, Phys. Rev. Lett. **87**, 187203 (2001).

[4] J. M. Hernández, F. Torres, J. Tejada, and E. Molins, Phys. Rev. B **66**, 161407(R) (2002); F. Torres, J. M. Hernandez, A. Garcia-Santiago, J. Tejada, and E. Molins, J. Magn. Magn. Mater. **272-276**, 1111 (2004).

[5] A. Cornia, R. Sessoli, L. Sorace, D. Gatteschi, A. L. Barra, and C. Daiguebonne, Phys. Rev. Lett. **89**, 257201 (2002).

[6] S. M. J. Aubin, Z. Sun, I. Guzei, A. Rheingold, G. Christou, and D. N. Hendrickson, Chem. Commun. (Cambridge) **1997**, 2239 (1997); Z. Sun, D. Ruiz, E. Rumberger, Ch. D. Incarvito, K. Folting, A. L. Rheingold, G. Christou, and D. N. Hendrickson, Inorg. Chem. **37**, 4758 (1998); D. Ruiz, Z. S. Sun, B. Albela, K. Folting, J. Ribas, G. Christou, and D. N. Hendrickson, Angew. Chem., Int. Ed. **37**, 300 (1998); D. Ruiz, Z. Sun, S. M. J. Aubin, E. Rumberger, C. Incarvito, K. Folting, A. L. Rheingold, G. Christou, and D. N. Hendrickson, Mol. Cryst. Liq. Cryst. **335**, 413 (1999).

[7] M. Soler, W. Wernsdorfer, Z. M. Sun, J. C. Huffman, D. N. Hendrickson, and G. Christou, Chem. Commun. (Cambridge) **2003**, 2672 (2003).

[8] K. Takeda, K. Awaga, T. Inabe, A. Yamaguchi, H. Ishimoto, T. Tomita, H. Mitamura, T. Goto, N. Mori, and H. Nojiri, Phys. Rev. B **65**, 094424 (2002).

[9] D. Ruiz-Molina, M. Mas-Torrent, J. Gomez, A. I. Balana, N. Domingo, J. Tejada, M. T. Martinez, C. Rovira, and J. Veciana, Adv. Mater. **15**, 42 (2003); J. Gómez-Segura, J. Veciana, and D. Ruiz-Molina, Chem. Commun. (Cambridge) **2007**, 3699 (2007), and references therein.

[10] I. Imaz, F. Luis, Ch. Carbonera, D. Ruiz-Molina, and D. Maspoch, Chem. Commun. (Cambridge) **2008**, 1202 (2008); C. Carbonera, I. Imaz, D. Maspoch, D. Ruiz-Molina, and F. Luis, Inorg. Chim. Acta **361**, 3951 (2008).

[11] J. Jung and M. Perrut, J. Supercrit. Fluids **20**, 179 (2001).

[12] M. Muntó, J. Gómez-Segura, J. Campo, M. Nakano, N. Ventosa, D. Ruiz-Molina, and J. Veciana, J. Mater. Chem. **16**, 2612 (2006).

[13] M. Gimeno, N. Ventosa, J. Veciana, Y. Boumghar, J. Fourier and I. Boucher, J. Supercrit. Fluids **38**, 94 (2006).

[14] H. Maruyama, J. Synchrotron Radiat. **8**, 125 (2001).

[15] D. E. Sayers and B. A. Bunker, in *X-Ray Absorption: Principles, Applications, Techniques of EXAFS, SEXAFS, XANES*, edited by R. Prins and D. Koningsberger (J. Wiley & Sons, New York, 1988), Chap. 6.

[16] K. Takeda, K. Awaga, and T. Inabe, Phys. Rev. B **57**, R11062 (1998).

[17] C. R. Natoli, in *EXAFS and Near Edge Structure*, edited by A. Bianconi, L. Incoccia, and S. Stipcich (Springer-Verlag, Berlin, 1983), p. 43.

[18] M. Benfatto, Y. Joly, and C. R. Natoli, Phys. Rev. Lett. **83**, 636 (1999); J. Chaboy, J. Synchrotron Radiat. (to be published).

[19] See, e.g., S. M. J. Aubin, Z. Sun, E. M. Rumberger, D. N. Hendrickson, and G. Christou, J. Appl. Phys. **91**, 7158 (2002) for Mn_{12} with FR and SR species; A. Sieber, R. Bircher, O. Waldmann, G. Carver, G. Chaboussant, H. Mutka, and H. U. Güdel, Angew. Chem., Int. Ed. **44**, 4239 (2005); E. M. Rumberger, E. del Barco, J. Lawrence, S. Hill, A. D. Kent, L. N. Zakharov, A. L. Rheingold, and D. N. Hendrickson, Polyhedron **24**, 2557 (2005), and references therein.

[20] See, e.g., E. del Barco, A. D. Kent, S. Hill, J. M. North, N. S. Dalal, E. M. Rumberger, D. N. Hendrickson, N. Chakov, and G. Christou, J. Low Temp. Phys. **140**, 119 (2005), and references therein.

[21] A. Bencini, I. Ciofini, and M. G. Uytterhoeven, Inorg. Chim. Acta **274**, 90 (1998).

[22] A. L. Barra, D. Gatteschi, R. Sessoli, G. L. Abbati, A. Cornia, A. C. Fabretti, and M. G. Uytterhoeven, Angew. Chem., Int. Ed. **36**, 2329 (1997).

[23] S. Hill, N. Anderson, A. Wilson, S. Takahashi, K. Petukhov, N. E. Chakov, M. Murugesu, J. M. North, E. del Barco, A. D. Kent, N. S. Dalal, and G. Christou, Polyhedron **24**, 2284 (2005).

[24] K. Park, M. R. Pederson, T. Baruah, N. Bernstein, J. Kortus, S. L. Richardson, E. Del Barco, A. Kent, S. Hill and N. S. Dalal, J. Appl. Phys. **97**, 10M505 (2005).

[25] F. Luis, J. Bartolomé, and J. F. Fernández, Phys. Rev. B **57**, 505 (1998); J. F. Fernández, F. Luis, and J. Bartolomé, Phys. Rev. Lett. **80**, 5659 (1998).

[26] A. L. Barra, D. Gatteschi, and R. Sessoli, Phys. Rev. B **56**, 8192 (1997).